NRIAG Journal of Astronomy and Geophysics (2013) 2, 54–66

National Research Institute of Astronomy and Geophysics

NRIAG Journal of Astronomy and Geophysics

www.elsevier.com/locate/nrjag

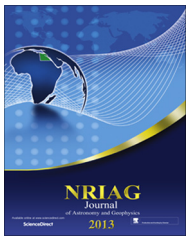

Discrimination between landmine and mine-like targets using wavelets and spectral analysis

Mahmoud A. Mohana [a], Abbas M. Abbas [a], Mohamed L. Gomaa [b], Shereen M. Ebrahim [a,*]

[a] *National Research Institute of Astronomy and Geophysics, Helwan, Cairo, Egypt*
[b] *Faculty of Engineering, Benha University, Shobra, Cairo, Egypt*

Received 23 October 2012; accepted 30 January 2013
Available online 25 July 2013

KEYWORDS

Ground penetrating radar (GPR);
Wavelets;
Spectrogram;
Finite difference time domain method (FDTD);
Landmine;
Mine-like

Abstract Landmine is an explosive apparatus hidden in or on the ground, which blows up when a person or vehicle passes over it. Egypt is one of the countries suffering due to the unexploded ordnance (UXO). Around 2 million UXO are present in the Egyptian soil especially at Al-Alameen province, north of the western desert. Detection of buried landmines is a problem of military and humanitarian importance.

Ground penetrating radar (GPR) is a powerful and non-destructive geophysical approach with a wide range of advantages in the field of landmine inspection. In the present paper, we apply different simulation models with Vivaldi antenna and mine-like targets by using the CST Microwave studio program. The field work is carried out by using a GPR device of model SIR 2000 from GSSI (Geophysical Survey Systems Incorporation) connected to 900 MHz antenna where the targets were buried in sand soil. Depending on the fact that the receiving powers (reflected, refracted and scattered) from the different materials are different, we study the spectral power densities for the received power from the different targets. The techniques used in this study are: direct fast Fourier transform, short time Fourier transform (spectrogram), wavelets transform and denoising techniques. Our results ought to be considered as finger prints for different scanned targets during this work. So we can discriminate between landmines and mine-like targets.

1. Introduction

Ground penetrating radar (GPR) is a geophysical instrument that uses radar pulses to image the subsurface of the earth. It involves the application of high frequency electromagnetic field (frequency band is 10–4000 MHz) to the ground. Its nature as a non-destructive technique in addition to its capability to allocate the fine targeted physical discrepancies enhances the chance to achieve progress in the field of landmine detection.

* Corresponding author. Tel.: +20 1220628558.
E-mail address: sherinmohamed2001@yahoo.com (S.M. Ebrahim).

Peer review under responsibility of National Research Institute of Astronomy and Geophysics.

ELSEVIER Production and hosting by Elsevier

2090-9977 © 2013 Production and hosting by Elsevier B.V. on behalf of National Research Institute of Astronomy and Geophysics.
http://dx.doi.org/10.1016/j.nrjag.2013.06.009

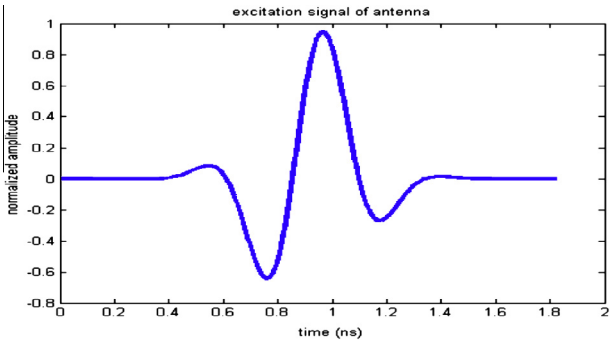

Fig. 1 Excitation signal of antenna.

Furthermore, its sensitivity to detect discontinuities in the electric permittivity of the ground has long been recognized as making it useful for finding landmines with little or no metal content (Daniels, 1996).

Several signal processing approaches have been suggested to improve the performance of GPR systems such as wavelets (Carevic, 1999), deconvolution (Roth, 2004) and spectrogram analysis. It is proven that, the use of the cross-correlation approach is faster in operation to locate the mine-like objects (Abbas and Lethy, 2005). The finite difference time domain (FDTD) method Yee, 1966 is one of the most popular techniques for the simulations of GPR problems (Daniels, 1996) and (Lawrence, 1998). The FDTD method has the power of

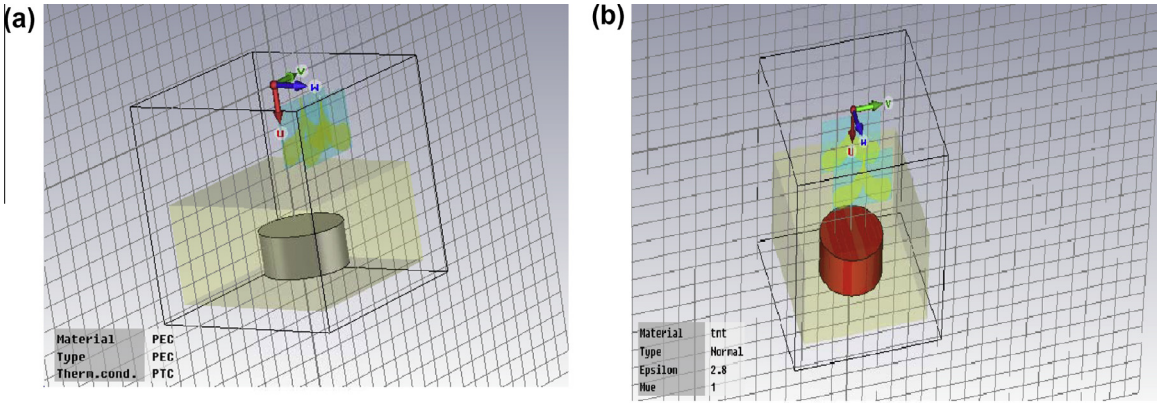

Fig. 2 models in CST program. (a) PEC model at a distance of 5.8 cm. (b) TNT model at a distance of 5.8 cm.

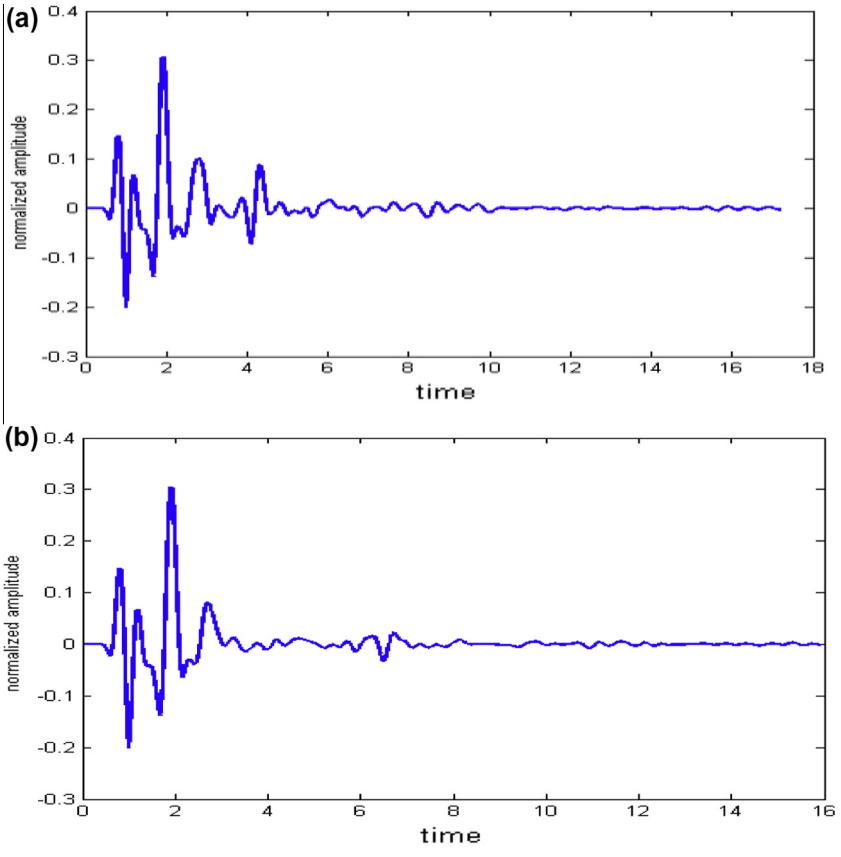

Fig. 3 GPR trace.

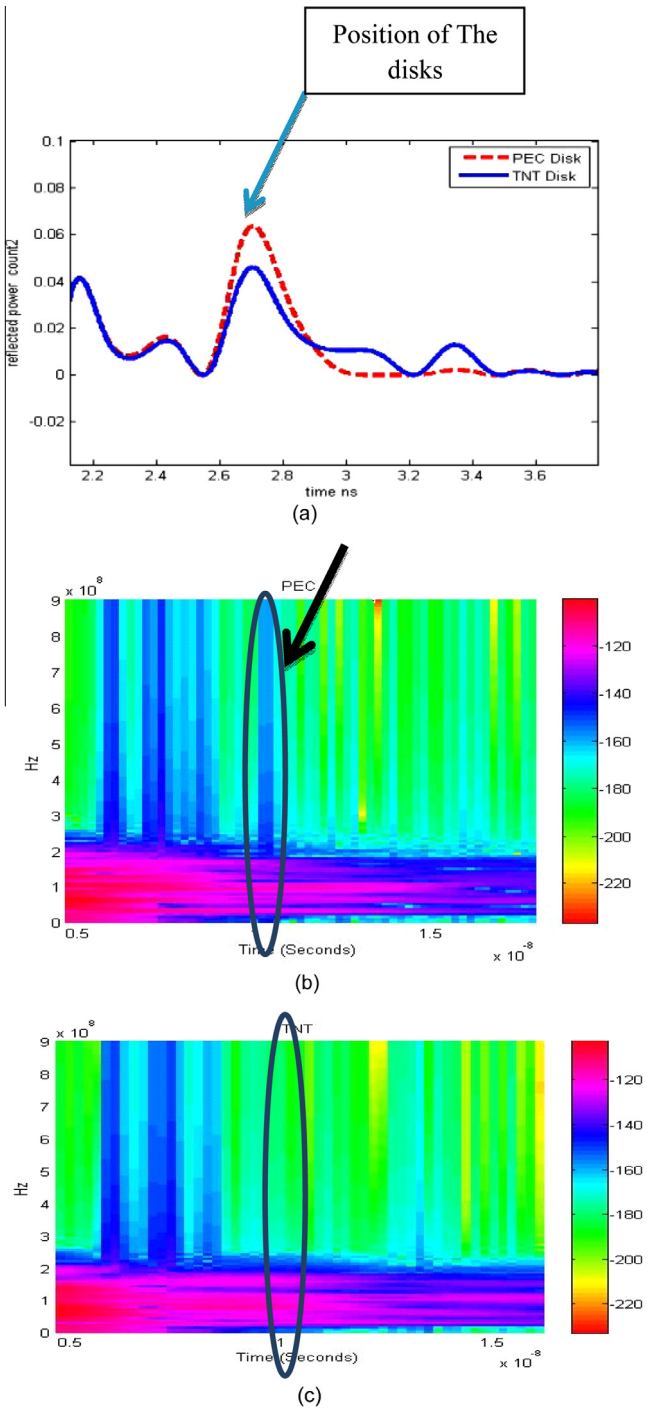

Fig. 4 Reflected power comparison and spectrogram analysis for PEC and TNT. (a) Reflected power comparison. (b) Spectrogram analysis of PEC. (c) Spectrogram analysis of TNT.

solving problems involving the arbitrarily layered media containing arbitrary inhomogeneities.

Detection algorithms are developed and used to discriminate between the buried targets and other inhomogeneities embedded in the ground. Hence, if the simulation results are to be used in the development of the detection algorithm, the heterogeneous nature of the ground should be included in the simulation model (Levent and Oğuz, 2001). This paper deals with using of CST Microwave Studio 2010 program (Manual of CST Microwave Studio, 2010) to generate different simulation models by using two Vivaldi antennas (Sato et al., 2004): one as a transmitter and the other as a receiver. Also TNT disk and metal disk targets buried in soil have been used. Significantly, an ultimate objective of this work, is to produce a scheme finger print for the different experimental targets coming here; initially the reflected signal power of the different targets is plotted in correspondence to their position. Then, spectrogram analysis, the Daubechies (db2) wavelets

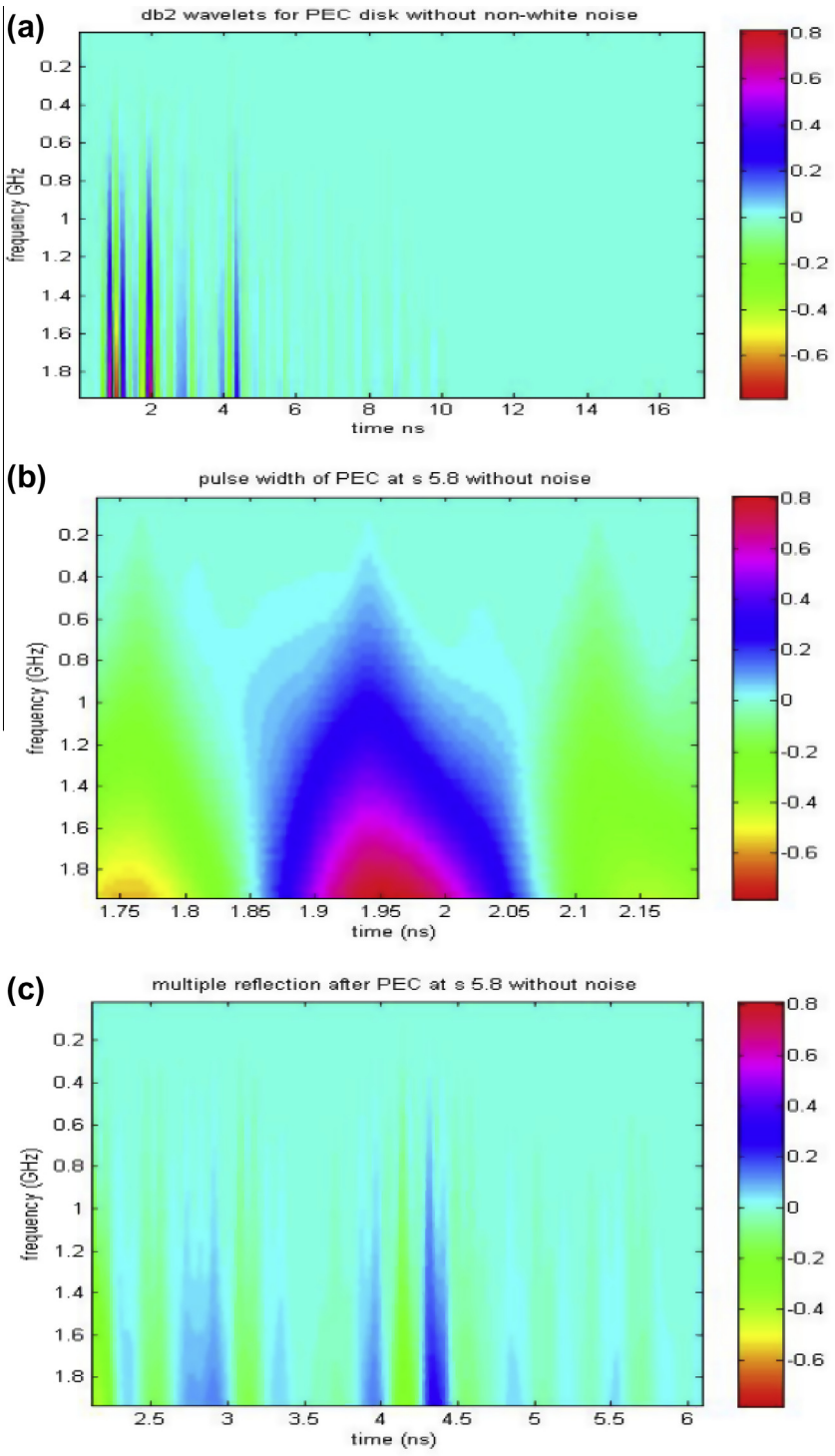

Fig. 5 PEC disk at a distance of 5.8 cm. (a) Db2 wavelets analysis after denoising. (b) Finger print of PEC disk. (c) Multiple reflections after PEC disk.

transform and denoising of non-white noise have been used to clarify the received signal from the individual targets. So it becomes possible to compare the physical scattering of each target and attribute it as the target's finger print.

Furthermore, experimental field work is carried out by using GPR of model SIR 2000 from GSSI attached to the antenna of 900 MHz to fulfill the conceptual assessments to validate the finger print assigning. Therefore; a test site has been constructed within the campus of the National Research Institute of Astronomy and Geophysics (NRIAG). The elaborations of the actual field work have been performed using four different itemized targets; plastic sphere, metal spheres, anti-tank landmine, and antipersonnel landmines. The used landmines are passive; the wick is demilitarized, they together

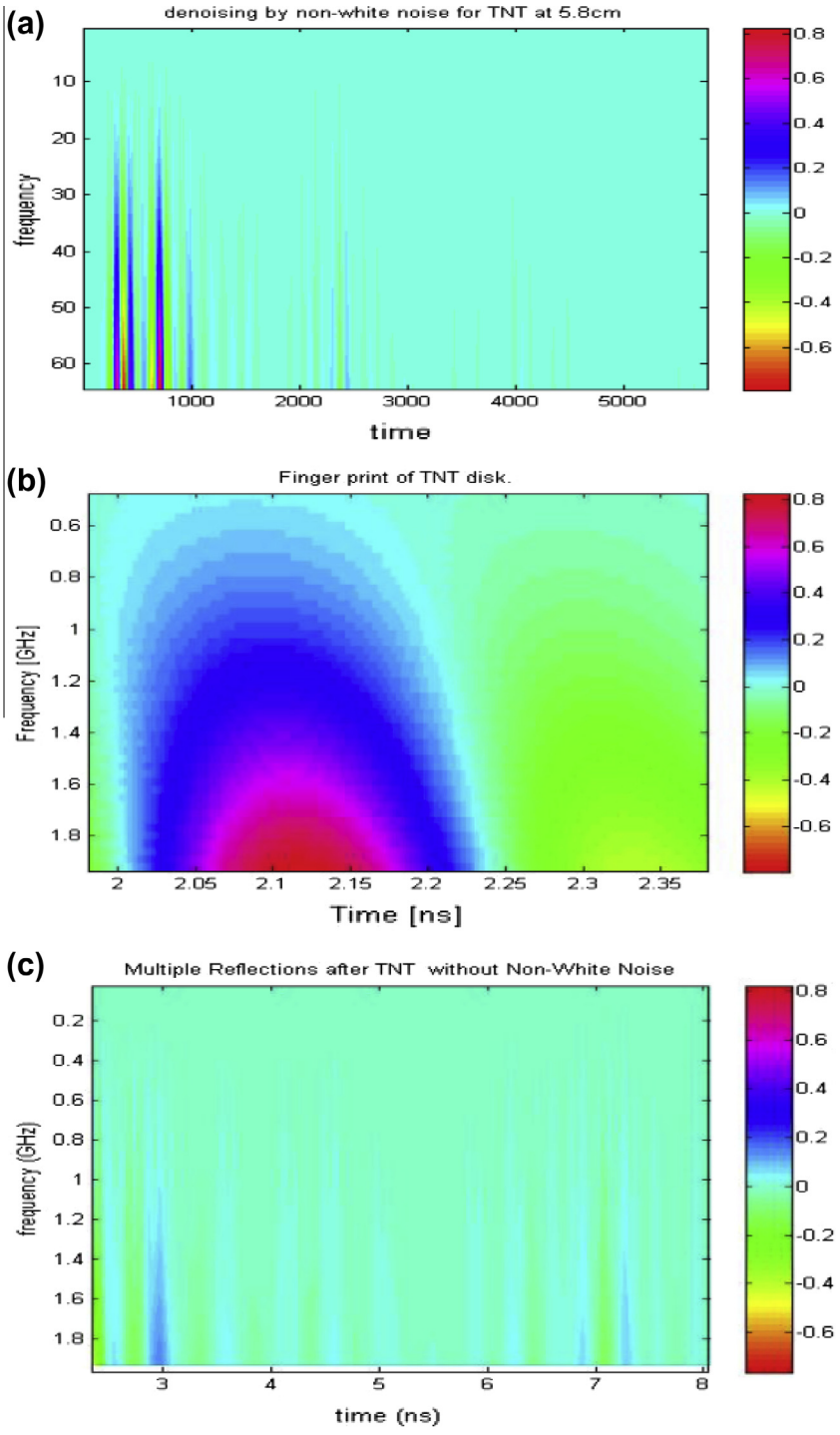

Fig. 6 TNT disk at a distance of 5.8 cm. (a) Db2 wavelets analysis after denoising. (b) Finger print of TNT disk. (c) Multiple reflections after TNT disk.

with the plastic and metal targets are buried in the sandy ground. Fitting curves have been made where the velocity of EM propagation could be estimated. The power distribution around the position of targets at wavelets and denoising of non-white noise have been studied, also the distribution of reflected power coming from the multiple reflections after targets positions have been made.

2. Simulation models

In this section, we carry out simulation models by using CST Microwave Studio 2010 program applying (FDTD) method, where two Vivaldi antennas separated by 5.8 cm distance are used as the transmitter (T_x) and the receiver (R_x) antennas. They operate in the radar frequency range between 100 MHz

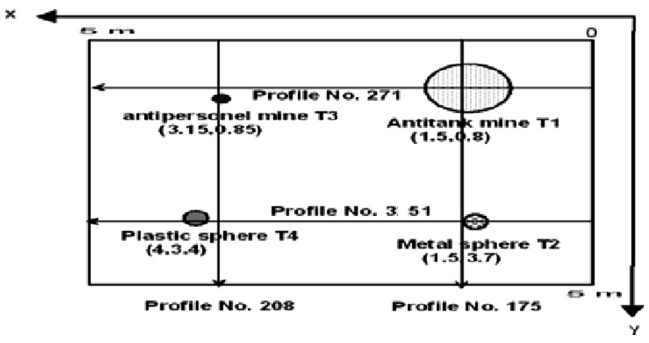

Fig. 7 The distribution of targets in the test site.

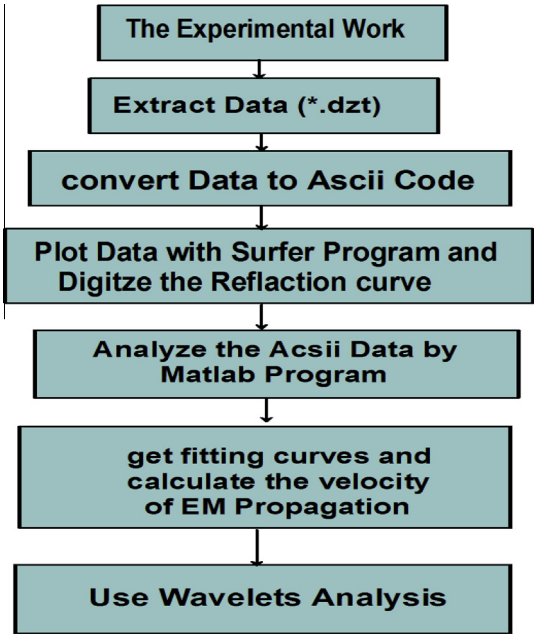

Fig. 8 The block diagram for work steps.

and 4 GHz. The excitation signal of the T_x antenna is shown in Fig. 1. Perfect electric conductivity (PEC) disk target and TNT disk target with assumed relative permittivity of 2.8 of radii of 10 cm, and heights of 10 cm are buried in the soil at a depth of 10 cm as shown in Fig. 2a and b. A relative permittivity of the soil is assumed to be 4 which imposed because it rewards the average relative permittivity of sand.

After the simulation run by the CST, we get the simulated reflection signal of disks as an ASCII code, and then we design a MATLAB routine to interpret these codes as shown in Fig. 3a and b. MATLAB calculates and plots the comparison of the reflected power of PEC disk, TNT disks, and the spectrogram image of the reflected signals which reveal the position and existence of the PEC and TNT disks as shown in Fig. 4a–c. Daubechies wavelets (db2) analysis Carevic, 1991 is implemented to sample the reflection signal produced in the CST output ASCII codes, the sampling period is 1 s along the sampling range 1 s as minimum and 64 s as the maximum with 1 s interval at each step (step by step mode). After analyzing the signal, we get 3D figures where the horizontal axis is the time, the vertical axis is the frequency and the color is the strength of the power content as shown in Figs. 5a and 6b. By comparing the Figs. 5 and 6, as a, b, and c correspondingly at the time which indicated from power Fig. 4a we find that the power distribution around this time looks like an inverted cup in all the studied cases as shown in Figs. 5b and 6b. The value of the area enclosed under this cup varies depending on the target kind, which has enabled us to differentiate between the metallic and non-metallic targets.The quantity of power under the cup equals $= \iint e(w,t)\mathrm{d}w\mathrm{d}t$, where e represents the power density at the point (w,t). Considering e is approximately constant all over the area under the cup, the approximate power can be equal $= e\iint \mathrm{d}w\mathrm{d}t$. Since the degree of color under the two cups of the two considered cases is approximately equal, we can use the areas under the two cups in comparison. Larger area indicates larger power distribution. The distribution of the reflected power coming from multiple reflections in the time phase which is located after the target position in the graph varies according to its kind. The ratio between multiple reflections after PEC disk is larger than multiple reflections after TNT disk. From these results we find that the TNT disk has a smaller area around the cup than the PEC disk as a result of high scattered power from the TNT disk. Also the area of multiple reflections for PEC is much wider than the area for TNT target. So we can use these results as finger print for targets.

3. Field test work

A test site has been carefully constructed in a soil-field comparable to the actual desert soil-field in which the UXO are distributed in Egypt; namely the Al-Alamein mine field, north of the western desert. An area of 5 m by 5 m in the NRIAG's campus has been selected for this purpose. We kept the land as much as possible undisturbed at its original site, so we tightly dug out soil to plant four test targets in the site, carefully marked, at a depth of 10 cm. The target set is composed of two actual mines brought in their passive form and two mine like targets; these are an antitank mine T_1, metallic sphere T_2, antipersonnel mine T_3, and plastic sphere T_4 and are distributed over the site as shown in Fig. 7. The site has been surveyed using the GPR instrument of model SIR 2000 from GSSI and monostatic antenna of 900 MHz. The interval

Table 1 The description of buried targets.

No.	Targets	Width (cm)	Height (cm)	Depth (cm)
1	Antitank mine	32	7	10
2	Metal sphere	9 cm diameter		10
3	Antipersonnel mine	7	6.8	10
4	Plastic sphere	9 cm diameter		10

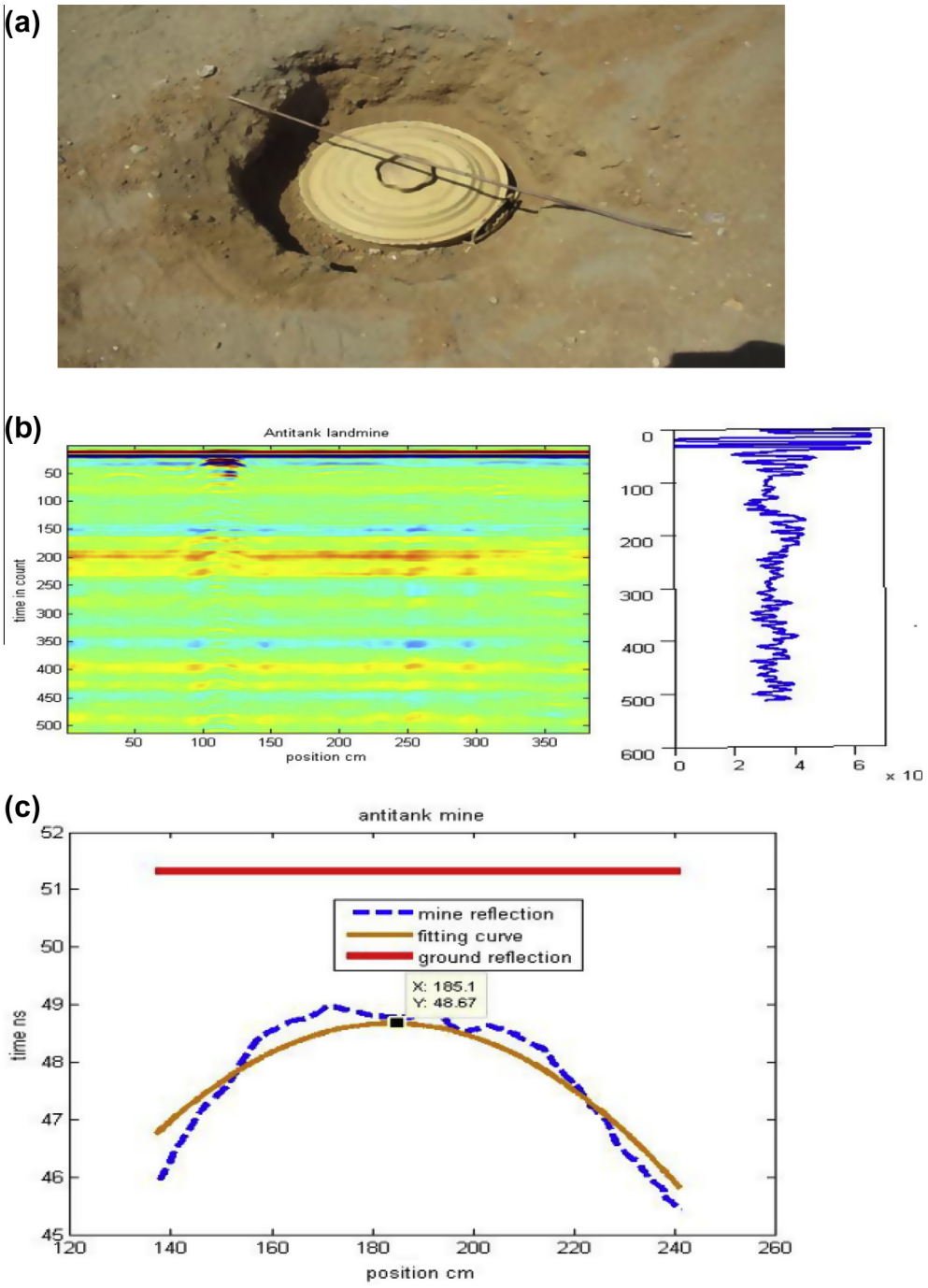

Fig. 9 Antitank mine T_1 results. (a) Photo of antitank mine. (b) GPR section and GPR trace. (c) Fitting curve.

between the successive GPR profiles was 5 cm. The continuous mode is used in this experiment. The GPR profiles cover the survey site in two perpendicular directions (x and y). Description of the used targets is shown in Table 1.

The experiment's work flow chart is shown as a block diagram in Fig. 8. The experimental work has been executed as described before, then the data are extracted from GPR instrument with Radan format (∗.dzt). The data are converted to ASCII code then treated by Surfer program which has to plot and digitize the curve The digitized data are analyzed by using MATLAB code to get fitting curves for all targets. The velocity of EM propagation in sand can be estimated respectively for the four targets by using the fitting curves as shown in Figs. 9a–c, 10a–c, 11a–c and 12a–c. We determine the depth of the targets (d) and found the time (T) from curves for target, and then we can calculate the velocity (v) by the equation

$$\left(v = \frac{2d}{T}\right)$$

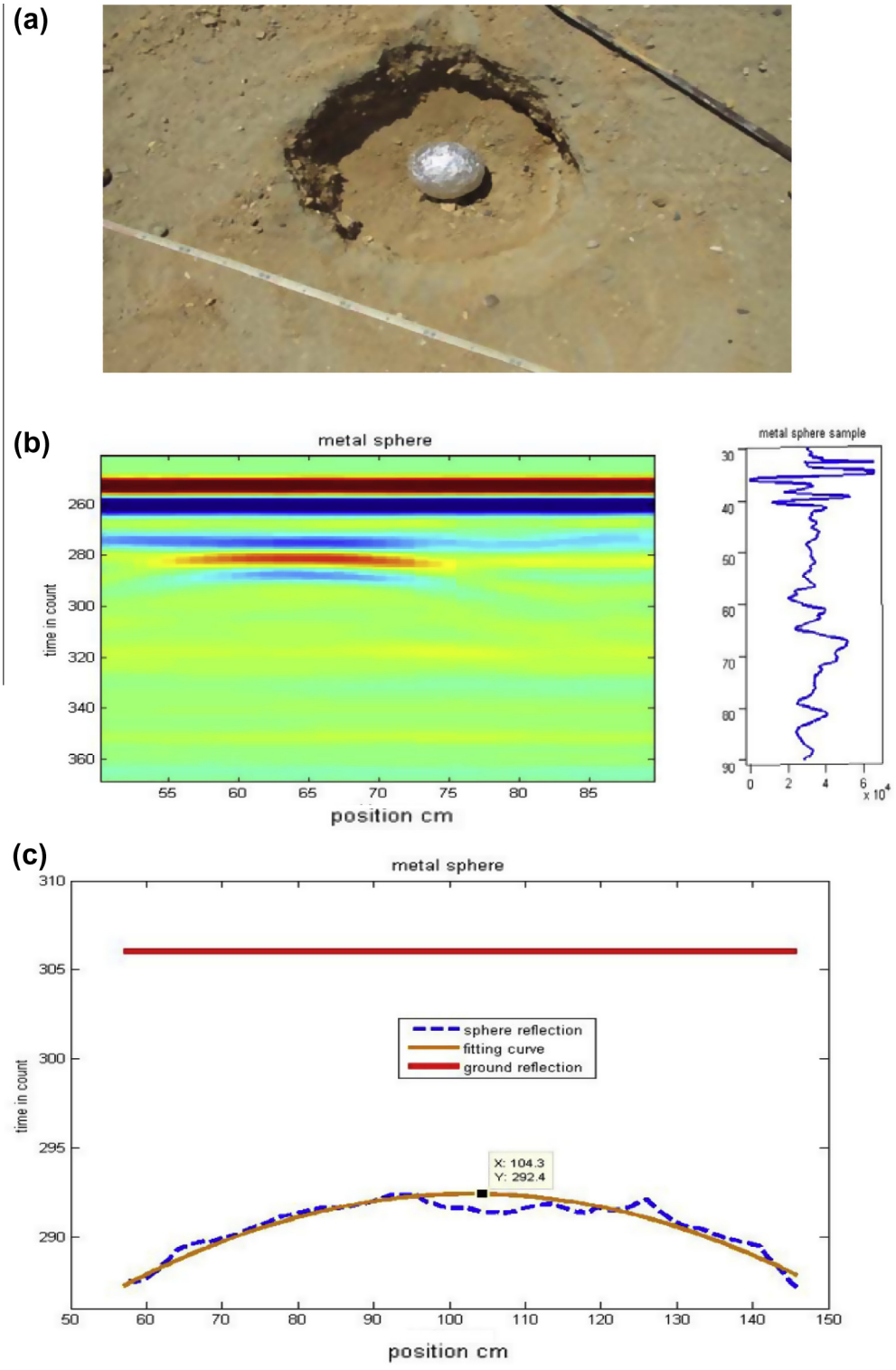

Fig. 10 Metallic sphere T_2 results. (a) Photo of metallic sphere. (b) GPR section and GPR trace. (c) Fitting curve.

From calculating we get that the velocities of EM propagation at all targets are 0.075, 0.075, 0.129 and 0.08 m/ns for Antitank, metallic sphere, antipersonnel and plastic sphere respectively. These velocities are nearby the velocity in between dry sand and saturated sand (wet sand) in Table 2 (Jol, 2009; Davis and Annan, 2009).

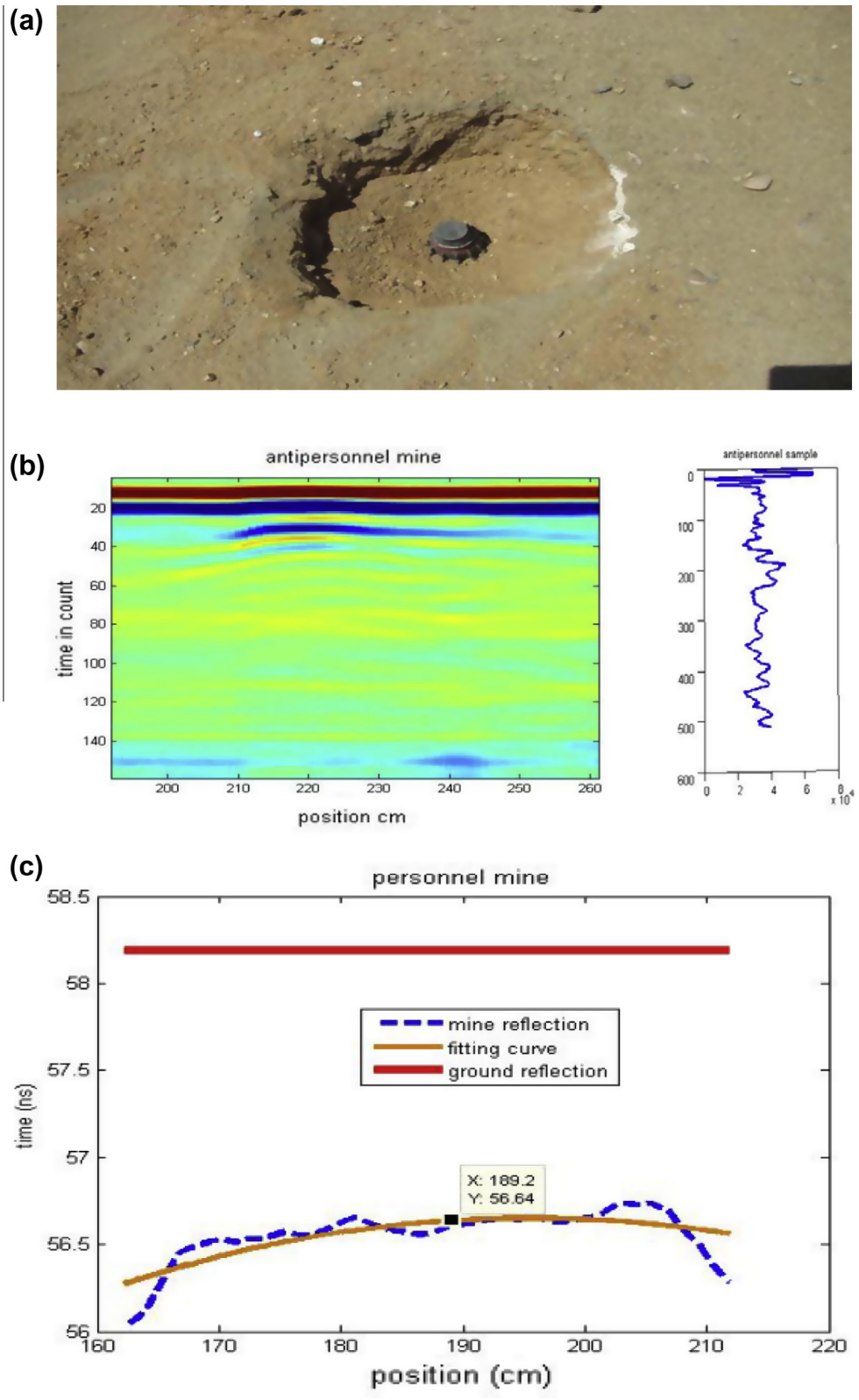

Fig. 11 Antipersonnel mine T_3 results. (a) Photo of antipersonnel mine. (b) GPR section and GPR trace. (c) Fitting curve.

Final step wavelets and denoising of non-white noise have been used to the trace the positions of targets where Fig. 13a–d shows the finger print for antitank, antipersonnel, metallic and plastic spheres respectively. From this figure we notice that every target has different power distribution around its position so that we could discriminate between

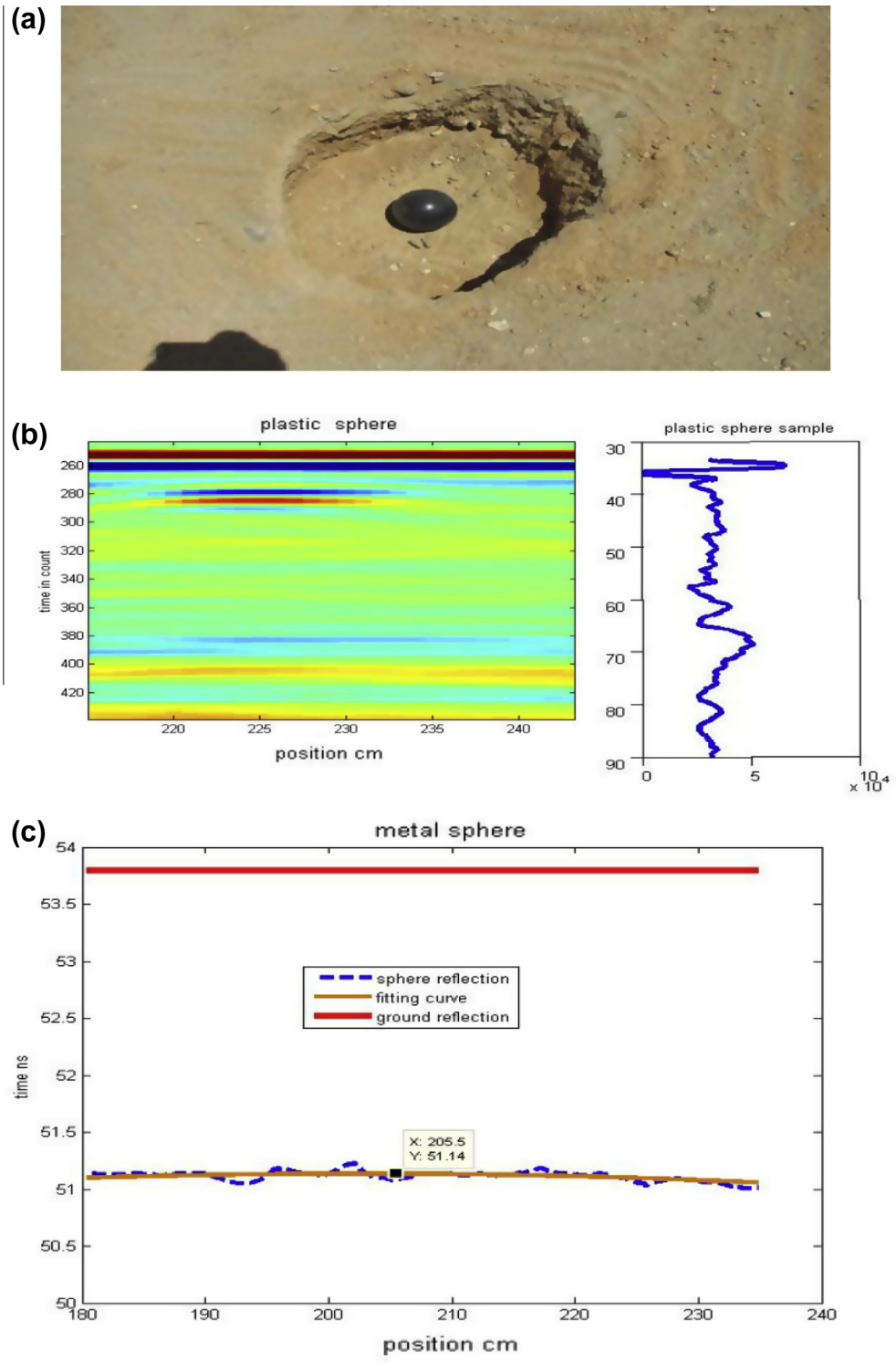

Fig. 12 Plastic sphere T_4 results. (a) Photo of plastic sphere. (b) GPR section and GPR trace. (c) Fitting curve.

them. Another way to discriminate between the targets is to study the distribution of power reflected as multiple reflections in the times which elapsed after the target position was determined. By comparing all multiple reflections we find that every target has different multiple reflections, where the multiple reflection after antitank is the strongest distribution power as shown in Fig. 14a–d.

4. Conclusion

In the present study, various techniques have been used to discriminate between two actual mines (brought in their passive state) and two mine-like targets. The simulation CST Microwave Studio 2010 program has been used to generate models

Table 2 Electrical properties of common geological media (Jol, 2009; Davis and Annan, 2009).

Material	ϵ_r	σ (mS/m)	v (m/ns)
Air	1	0	0.3
Distilled water	80	0.01	0.033
Fresh water	80	0.5	0.033
Sea water	80	30.00	0.01
Dry sand	3–5	0.01	0.15
Saturated sand	20–30	0.1–1.0	0.06
Limestone	4–8	0.5–2	0.12
Shale	5–15	1–100	0.09
Silt	5–30	1–1000	0.07
Clay	4–40	2–1	0.06
Granite	4–6	0.01–1	0.13
Salt (dry)	5–6	0.01–1	0.13
Ice	3–4	0.01	0.16

ϵ_r: the dielectric constant.
σ: the electrical conductivity of medium (m Siemens/m).
v: the velocity of the electromagnetic wave in medium.

for condition of mines (metal, TNT disks) buried in the subsoil at a depth of 10 cm. Our approach is to get initially the target positions by comparing the reflected power. Then we use the Daubechies wavelets (db2) and spectrogram to compare between the metal PEC and TNT disks. By comparing two images one for the metal and another for the TNT under the same conditions, we find that the power distributions around the positions which were determined from reflected power figures look like inverted cups in all cases. The calculated areas under these inverted cups are differing from one target to another. The areas representing multiple reflections are different also. So we easily differentiate between two targets by using the last information as a finger print for targets.

The field work and MATLAB code has been used to get fitting curves for the relation between the position and depth of all the buried targets to estimate approximately the propagation velocity of the EM wave in the soil used in our experiment. The estimated velocities are close to the velocity of wet sand in reference tables. Also we use wavelets and denoising of non-white noise to make finger prints of targets by initially

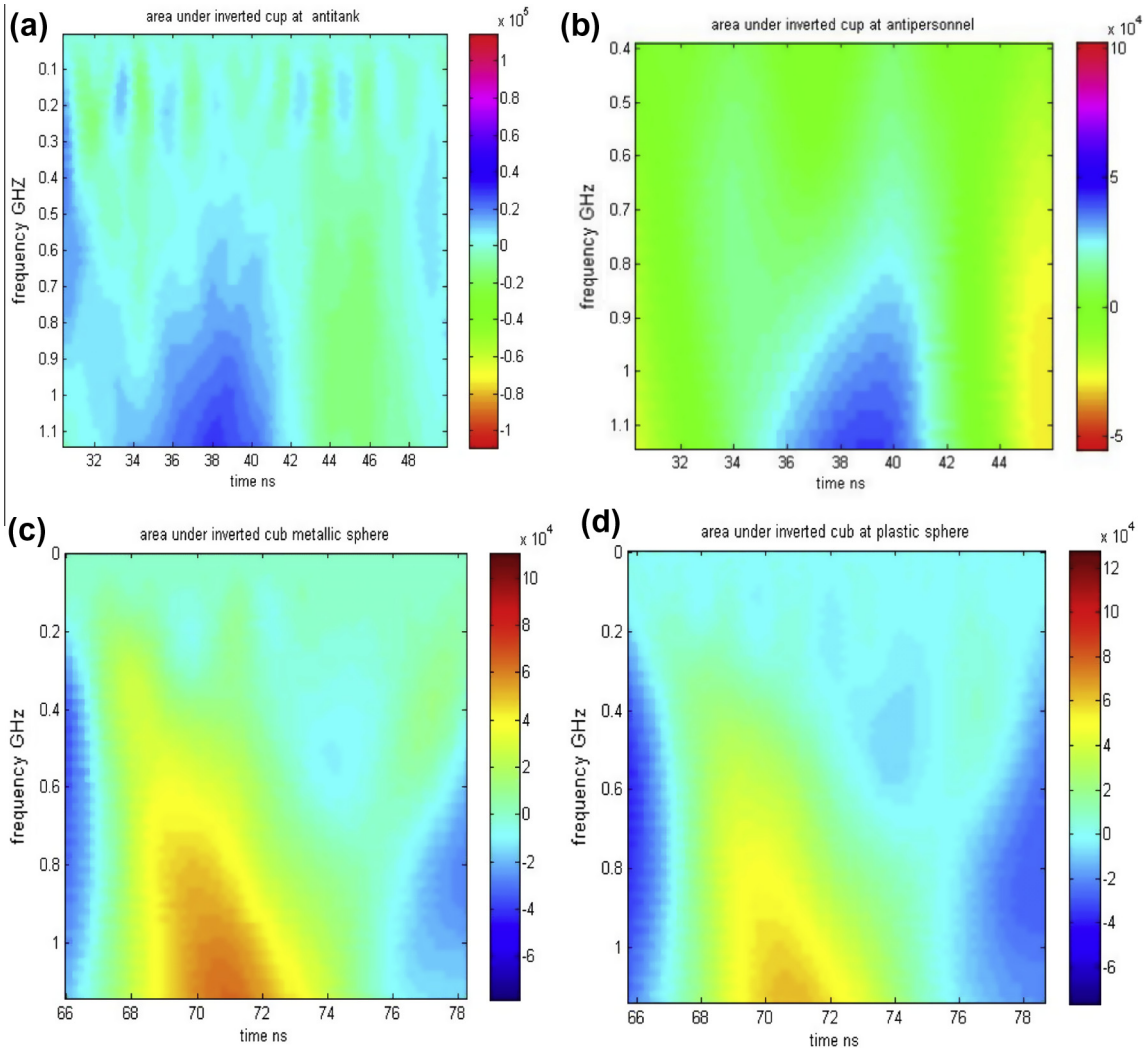

Fig. 13 Power distribution around the object. (a) Antitank mine. (b) Antipersonnel mine. (c) Metallic sphere. (d) Plastic sphere.

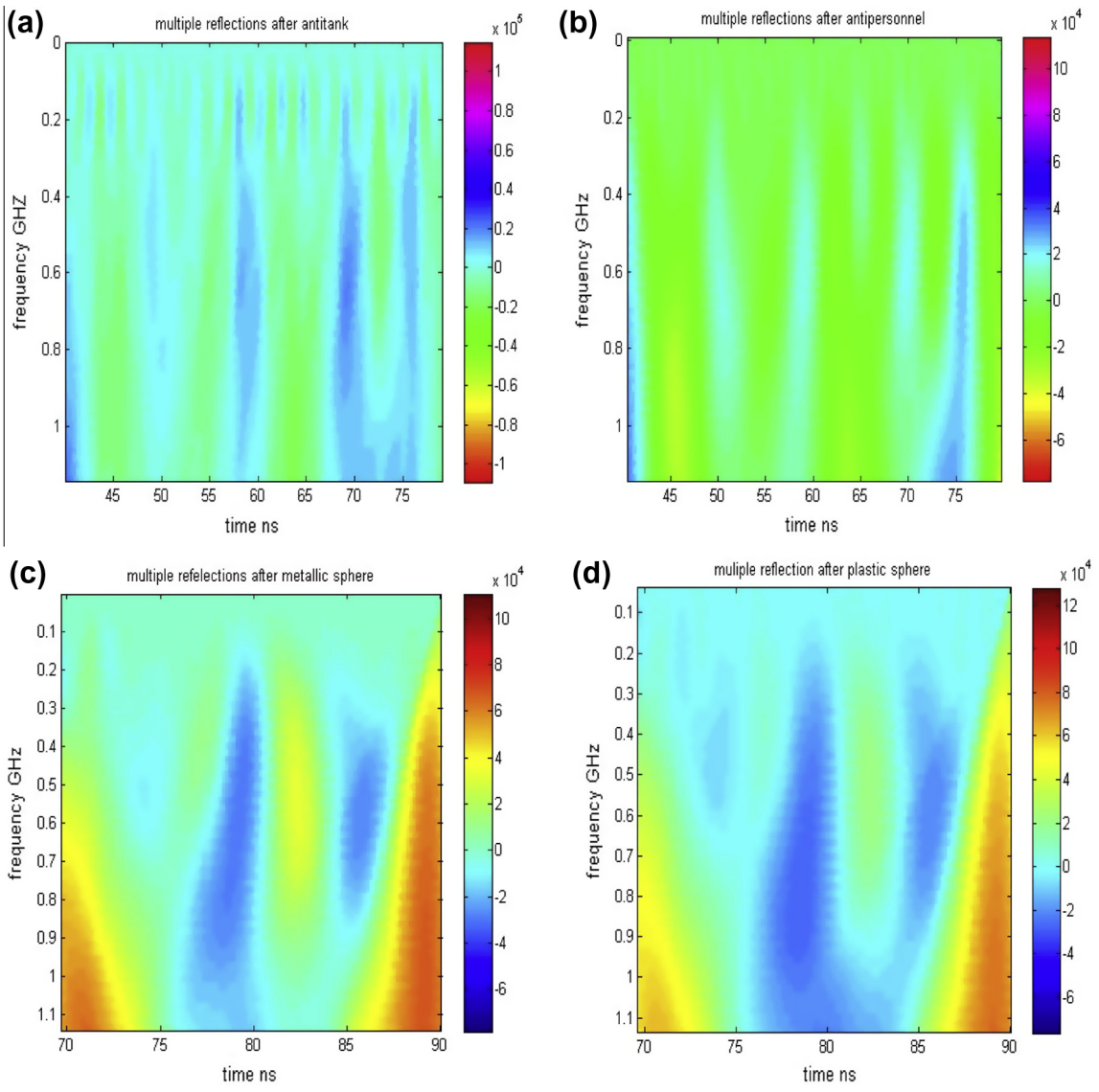

Fig. 14 Multiple reflections after positioning of targets. (a) Antitank mine. (b) Antipersonnel mine. (c) Metallic sphere. (d) Plastic sphere.

studying the reflected power distribution around the target which is similar to the shape of an inverted cup which varies depending on the target type. Then the distribution of power reflected as multiple reflections in the time phase which is elapsed after the target position in the graph varies according to its kind. These results enable us to discriminate between the characteristics of different targets.

Acknowledgement

The authors like to express their thanks to Prof. Dr. Hanafy Deebes and Prof. Dr. Hamed Nofal for reviewing the manuscript. Thanks are also extended to Prof. Dr. Magdy Atya, Dr Khamis Kabil and Dr. Mahmoud Gaballa for their participation in the data collection and data processing. Also, thanks are given to our colleagues from the Electrical and Geothermal laboratory that helped us clime the data acquisition.

References

Abbas, A.M., Lethy, A.M.Al., 2005. Implementation of wave-let correlation to locate landmine-like objects using GPR data as experimented on a test site. J. Coll. Petrol. Eng. Mining. 8 (2), 57–71.

Carevic, D., 1999. Clutter reduction and target detection in ground penetrating radar data using wavelets. In: Detection and Remediation Technologies for Mines and Mine-like Targets IV. Proceedings of the SPIE, vol. 3710. pp. 973–978.

Carevic, D., 1991. Wavelet-based method for detection of shallowly buried objects from GPR data. In: Proc. Information Decision and, Control. pp. 201–206.

Daniels, D.J., 1996. Surface-Penetrating Radar. IEE.

Davis, J.L., Annan, A.P., 2009. Ground-penetrating radar for high-resolution mapping of soil and rock stratigraphy. Geophys. Prospect. 37 (5).

Jol, M., 2009. Ground Penetrating Radar: Theory and Applications. Elsevier, Amsterdam.

Lawrence, K.S., 1998. Ground penetrating radar. In: 7th Int. Conf.
Levent, G., Oğuz, U., 2001. Simulations of ground-penetrating radars over lossy and heterogeneous grounds. IEEE Trans. Geosci. Remote Sens. 39 (6).
Manual of CST Microwave Studio, 2010.
Roth, F., 2004. Convolutional for Landmine Identification with Ground Penetrating Radar. Master thesis. Technische University Delft.
Sato, M., Hamada, Y., Feng, X., Kong, F., Zeng, Z., Fang, G., 2004. GPR using an array antenna for landmine detection. Near Surface Geophys., 3–9.
Yee, K.S., 1966. Numerical solution of initial boundary value problems involving Maxwell's equations in isotropic media. IEEE Trans. Antennas Propagat. 14, 302–307.